Inverse convection in a flat mini-channel: towards estimation of fluid bulk temperature distribution with infrared thermography

Yassine Rouizi, Denis Maillet, Yves Jannot, Isabelle Perry

HAL Id: hal-02321543
https://hal.science/hal-02321543

Inverse convection in a flat mini-channel: towards estimation of fluid bulk temperature distribution with infrared thermography

To cite this article: Yassine Rouizi *et al* 2012 *J. Phys.: Conf. Ser.* **395** 012070

View the article online for updates and enhancements.

Related content

- Parametric low-order models in transient heat diffusion by MIM. Estimation of thermal conductivity in a 2D slab
  Manuel Girault, Laurent Cordier and Etienne Videcoq

- Pressure drop and heat transfer characteristics for single-phase developing flow of water in rectangular microchannels
  Mirmanto, D B R Kenning, J S Lewis et al.

- Bouncing bubble dynamics and associated enhancement of heat transfer
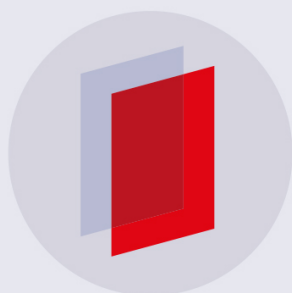 David B Donoghue, Yan M C Delauré, Abdulaleem Albadawi et al.

Inverse convection in a flat mini-channel: towards estimation of fluid bulk temperature distribution with infrared thermography

Yassine Rouizi, Denis Maillet, Yves Jannot and Isabelle Perry

Laboratoire d'Energétique et de Mécanique Théorique Appliquée LEMTA, Université de Lorraine et CNRS, 2, avenue de la Forêt de Haye - 54504 Vandoeuvre-lès-Nancy cedex - France

E-mail: `yassine.rouizi@ensem.inpl-nancy.fr` `denis.maillet@ensem.inpl-nancy.fr`
`yves.jannot@ensem.inpl-nancy.fr` `isabelle.perry@ensem.inpl-nancy.fr`

Abstract. This study deals with the solution of an inverse problem in a flat mini-channel of of 1 mm thickness. At this scale, the difficulty is to introduce non-intrusive sensors. The sensors can modify the local flow and therefore the heat transfer. Our objective is to characterize the mean velocity U and the heat transfer coefficient of external exchange h in order to recover the bulk temperature distribution $T_b(x)$. The inverse method makes it possible to go back to this information starting from measurement of the temperature fields on the two external faces of the channel and from a corresponding model through the minimization of a least square criterion. In this work, the temperature fields can be obtained either by a numerical model or by infrared thermography. Before an experimental validation by infrared thermography, we perform numerical simulations and a sensitivity analysis of the external temperature fields to the mean flow velocity U and to the external heat transfer coefficient h. The temperature and flux distributions over the internal faces of the walls are estimated by an inverse method then.

1. Introduction

Modelling fluid flow and heat transfer inside a mini- or micro-channel constitutes a challenge because it requires taking into account many effects that do not occur in traditional macro-structured systems [1]. In a mini-channel, presence of solid walls, whose volume fraction is not negligible, modifies heat transfer and can induce axial conduction effects in the channel walls. These are generally neglected in the macro-systems [2, 3].

This study concerns the numerical and experimental modelling of both single phase water flow and heat transfer (conduction and advection) in a flat mini-channel (see figure 1). The flowing fluid layer (1 mm thickness) is located between two parallel polycarbonate solid walls (1 and 2 mm thicknesses). This material has been chosen in order to minimize axial conduction. In mini-channel heat exchangers, it provides higher effectivenesses than good conductors such as copper [2]. The objective of this paper lies in the inversion of the recorded temperature fields on the external faces of this plane channel, which can be measured using an infrared camera, as well as a model of conjugated transfer [4] in the three layers of the system (two walls and the layer of the flow), for :

- estimating the structural parameters of this thermal system (mean velocity and external heat transfer coefficient)

- recovering the temperatures of internal walls and the corresponding wall fluxes from the external temperature distribution and from the external heat transfer coefficient estimated previously.

2. The studied system and its modelling

Let us consider the following system (figure 1): a laminar flow in a channel of length $2L$ of thickness e_f, limited by two parallel polycarbonate plates of thicknesses e_1 and e_2. A velocity profile $u(y)$ and a temperature T_∞ are imposed at the entrance of the channel. Two uniform heat flux (φ_{hot} and φ_{cold}) are imposed on a portion $\ell = 12$ mm of the external faces. The remaining parts of these faces are subject to convective losses to the ambient environment, and the lateral faces are insulated, see Figure 1.
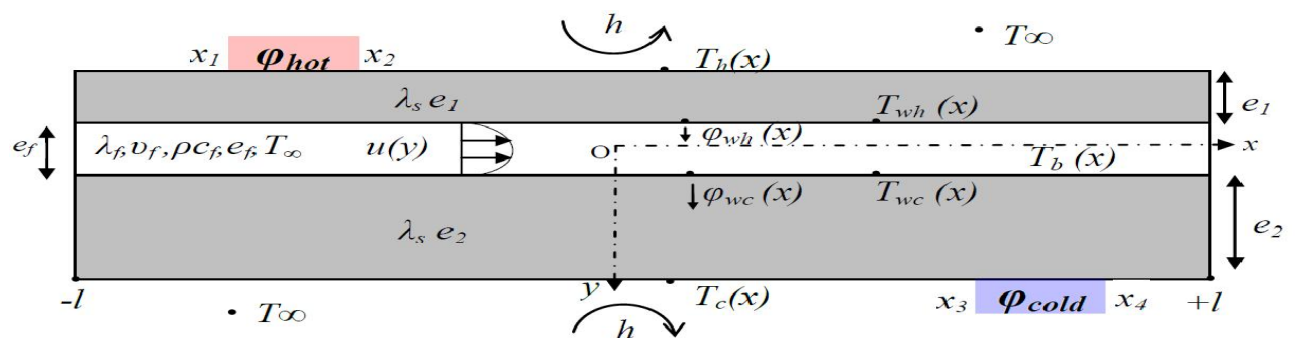

Figure 1. Geometry of mini-channel

The two solid plates are characterized by a thermal conductivity λ_s and a volumetric heat capacity ρc_s. The internal thickness is e_f and the fluid (water) is characterized by a conductivity λ_f, a volumetric heat capacity ρc_f and a kinematic viscosity ν_f.

2.1. Analytical model

The equations describing the steady state heat transfer in the mini-channel and in the adjacent parallel polycarbonate plates with the corresponding boundary conditions are given below:

- The heat equation in the walls:

$$\frac{\partial^2 T_s}{\partial x^2} + \frac{\partial^2 T_s}{\partial y^2} = 0 \quad (1)$$

- The heat equation in the fluid:

$$\lambda_f \left(\frac{\partial^2 T_f}{\partial x^2} + \frac{\partial^2 T_f}{\partial y^2} \right) - \rho c_f u(y) \frac{\partial T_f}{\partial x} = 0 \quad (2)$$

- Transverse boundary conditions on the external faces, where φ is the heat flux density and $\mathcal{H}$ is the Heaviside step function :

  - at $y = -e_f/2 - e_1$:

$$-\lambda_s \frac{\partial T}{\partial y} = \varphi_{hot} \left[\mathcal{H}(x - x_1) - \mathcal{H}(x - x_2) \right] - h(T - T_\infty) \quad (3)$$

  - at $y = +e_f/2 + e_2$

$$-\lambda_s \frac{\partial T}{\partial y} = -\varphi_{cold} \left[\mathcal{H}(x - x_3) - \mathcal{H}(x - x_4) \right] + h(T - T_\infty) \quad (4)$$

- Solid/fluid interface conditions at $y = \pm e_f/2$:

$$-\lambda_s \frac{\partial T_s}{\partial y} = -\lambda_f \frac{\partial T_f}{\partial y} \quad \text{and} \quad T_s = T_f \quad (5)$$

To find the solution of this problem, one can use the Fourier integral transform defined by:

$$\theta\left(\alpha_n, y\right) = \theta_n\left(y\right) = \int_{-L}^{+L} T\left(x, y\right) e^{-i\alpha_n x} dx \tag{6}$$

where $\alpha_n = \frac{n\pi}{L}$ is the discrete eigenvalue of order n that correspond to a virtual domain $[-L\ L]$ which includes the real $[-l\ l]$ interval corresponding to the channel shown in figure 1 $(L \geq l)$. We assume that $T_i = T_\infty$ and $\partial T_i/\partial x = 0$ at $x = -L$ for $i = s$ or f and that there is no heat source for $x \in [l\ L]$ which yields $T_i = T_\infty$ and $\partial T_i/\partial x = 0$ in $x = L$.

Before carrying out the development in Fourier domain of equations (1) and (2), and in order to make the velocity field $u\left(y\right)$ homogeneous in a set of K fluid sub-layers, the velocity in each layer of thicknesses $e_k = y_k - y_{k-1} = e_f/K$ corresponds to a constant velocity u_k:

$$u\left(y\right) = \frac{3}{2}U\left(1 - 4\left(\frac{y}{e_f}\right)^2\right) \quad \Rightarrow \quad u_k = \frac{3}{2}U\left(1 - \frac{4K}{3e_f^3}\left(y_k^3 - y_{k-1}^3\right)\right) \tag{7}$$

After the integral transformation, equations (1) and (2) can be written as follows [4, 5] :

• in the walls: \qquad\qquad\qquad\qquad\qquad\qquad • in the fluid:

$$\frac{\mathrm{d}^2\theta_s}{\mathrm{d}y^2} - \alpha_n^2\theta_s = 0 \qquad (8) \qquad\qquad\qquad \frac{\mathrm{d}^2\theta_f}{\mathrm{d}y^2} - \gamma_n^2\theta_f = 0 \qquad (9)$$

where $\gamma_n^2 = \alpha_n^2 + i\frac{u_k}{a_f}\alpha_n$ and $a_f = \frac{\lambda_f}{\rho c_f}$.

Introducing Φ as being the Fourier transform of the heat flux density φ with:

$$\varphi = -\lambda\frac{\partial T}{\partial y} \tag{10}$$

the general solution of equations (8) to (10) can be written in the quadrupoles form [4]:

$$\begin{bmatrix}\theta_n \\ \Phi_n\end{bmatrix}_h = \boldsymbol{H}_1\boldsymbol{S}_{1n}\left(\prod_{k=1}^{K}\left(\boldsymbol{F}_{kn}\right)\right)\boldsymbol{S}_{2n}\boldsymbol{H}_2\begin{bmatrix}\theta_n \\ \Phi_n\end{bmatrix}_c \tag{11}$$

where the subscripts h and c denote respectively the external hot face and the external cold face, and with

$$\boldsymbol{H}_1 = \boldsymbol{H}_2 = \begin{bmatrix}1 & 0 \\ h & 1\end{bmatrix}, \quad \boldsymbol{S}_{in} = \begin{bmatrix}A_{in} & B_{in} \\ C_{in} & A_{in}\end{bmatrix} \quad \text{and} \quad \boldsymbol{F}_{kn} = \begin{bmatrix}A_{kn} & B_{kn} \\ C_{kn} & A_{kn}\end{bmatrix} \tag{12}$$

and $A_{in} = \cosh\left(\alpha_n e_i\right)$, \quad $B_{in} = \sinh\left(\alpha_n e_i\right)/\left(\lambda_s\alpha_n\right)$ \quad and \quad $C_{in} = \left(\lambda_s\alpha_n\right)\sinh\left(\alpha_n e_i\right)$, \
$A_{kn} = \cosh\left(\gamma_n e_k\right)$, \quad $B_{kn} = \sinh\left(\gamma_n e_k\right)/\left(\lambda_f\gamma_n\right)$ \quad and \quad $C_{kn} = \left(\lambda_f\gamma_n\right)\sinh\left(\gamma_n e_k\right)$.

The temperature distribution $T\left(x, y\right)$ analytical solution of equations (1) and (2) is obtained through an inverse truncated Fourier transformation with N_h harmonics:

$$T(x, y) \approx \frac{1}{2L}\sum_{n=-N_h+1}^{N_h}\theta_n\left(y\right)e^{i\alpha_n x} \tag{13}$$

2.2. Numerical model: simulations for constant flux
At first, our objective is to use the temperature profiles on the external faces and the analytical model to estimate the mean velocity U and the external heat transfer coefficient h. Two types of simulations were carried out here to obtain the temperature fields . The first one uses the commercial code COMSOL [6], and the second presented above uses a quadrupoles model based on the development with Fourier transforms.

In figures (2) and (3), the temperature profiles on the external faces are plotted. They correspond to different mean velocities U (see table 1) and to the nominal values of the parameters of our model given in table 2.

U (m/s)	Re	Pe	M
10^{-3}	1.99	13.96	$4\ 10^{-3}$
10^{-4}	$1.99\ 10^{-1}$	1.396	$4\ 10^{-2}$
10^{-5}	$1.99\ 10^{-2}$	$1.396\ 10^{-1}$	$4\ 10^{-1}$

Table 1. Mean velocity and corresponding non-dimensional numbers.

Here Re and Pe are the Reynolds and Péclet numbers and M is the non-dimensional number introduced in [2] that quantifies the ratio of the heat flow rates transferred by axial conduction in the wall and convective heat transfer in the flow [2, 4]:

$$Re = \frac{2Ue_f}{\nu} \quad \text{and} \quad Pe = \frac{2Ue_f}{a_f} \quad \text{and} \quad M = \frac{\lambda_s e_s}{\rho c_f e_f\ \ell\ U} \tag{14}$$

h	φ_{hot}	φ_{cold}	T_∞	e_f	e_1	e_2	l
W.m^{-2}.K^{-1}	W.m^{-2}	W.m^{-2}	°C	m	m	m	m
10	275	-275	20	10^{-3}	10^{-3}	2.10^{-3}	6.10^{-2}

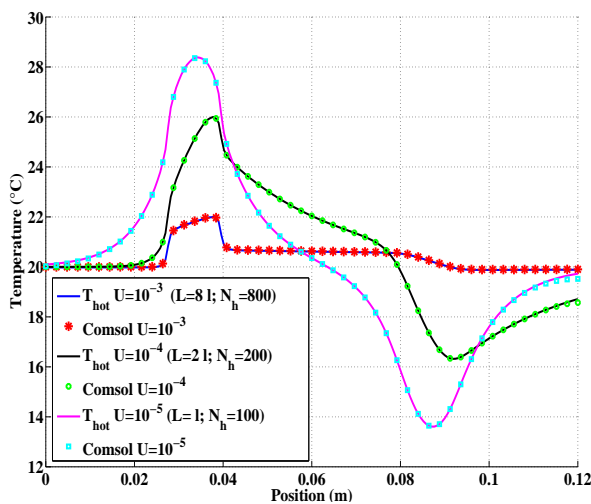**Table 2.** Standard parameters of our simulation.

Figure 2. Comparison analytical/numerical temperature on hot face for different mean velocities U.
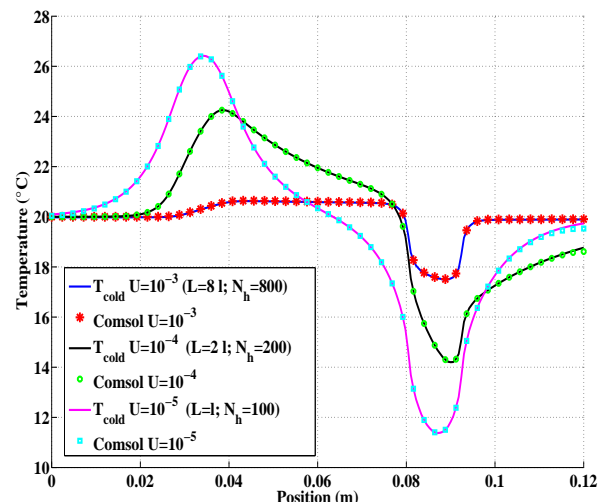
Figure 3. Comparison analytical/numerical temperature on cold face for different mean velocities U.

One notes in figures 2 and 3 the very good agreement between the temperature profiles calculated by COMSOL code [6] and those obtained by the analytical model. A small difference

appears at the downstream end of the channel: it can be explained by the short distances between the sources and the insulated ends.

3. Inverse approach

Our first objective is to use the temperature profile at one of the external faces to estimate both the mean velocity of the fluid U and the external heat transfer coefficient h. Before implementing this parameter estimation problem, a sensitivity study has been made for parameters U and h. The four scaled sensitivities on both external faces are given below:

$$S^*_{\text{hot}U} = U\frac{\partial T_h}{\partial U}, \quad S^*_{\text{cold}U} = U\frac{\partial T_c}{\partial U}, \quad S^*_{\text{hot}h} = h\frac{\partial T_h}{\partial h} \quad \text{and} \quad S^*_{\text{cold}h} = h\frac{\partial T_c}{\partial h} \tag{15}$$

These coefficients are plotted in figures (4) for different mean velocities U (10^{-5}, 10^{-4} and 10^{-3} (m/s)).
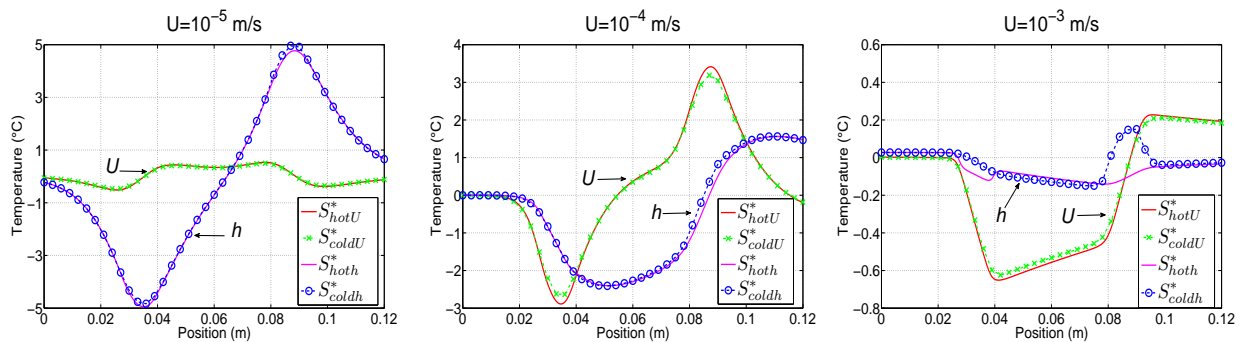

Figure 4. Distribution of scaled sensitivity for different value of U.

The scaled sensibilities on both external faces are almost same. For a low mean velocity U, the levels of the scaled sensitivity to the external heat transfer coefficient h are more important than those to the mean velocity U. On the contrary, the levels of scaled sensitivity to U become dominant for high velocities. We can conclude that the higher the velocity the higher advection prevails with respect to conduction in the heat exchange (see the Péclet number levels).

3.1. Estimation of U and h

For the first attempt of inversion we use the data without noise. The estimation is performed through the minimization of a quadratic criterion built on the difference between the analytical temperature profile on the hot face $T_h(x_i)$ for $U = 10^{-5}$ (m/s) and $h = 10$ (W.m^{-2}.K^{-1}) on $N_x = 200$ points equally spaced between $-l$ and l and the analytical model output $T_h(x_i; U, h)$:

$$\mathcal{J}(U,h) = \frac{1}{2}\sum_{i=1}^{N_x}\left(T_h(x_i) - T_h(x_i; U, h)\right)^2 \tag{16}$$

This procedure of minimization uses a method of nonlinear programming based on Trust region algorithm (MATLAB [7]).

For the lowest velocity case, one obtains after minimization $\hat{U} \approx 10^{-5}$ (m/s) and $\hat{h} \approx 10$ (W.m^{-2}.K^{-1}) with relative estimation errors of the order of 2.10^{-7} for U and 3.10^{-6} for h and with a mean quadratic error $\sigma = \sqrt{\mathcal{J}/N_x} = 2.6\ 10^{-5}$ K. Then, one adds a normal and independent noise to the temperature profile $T_h(x)$. This noise is characterized by a standard deviation

$\sigma_T = 0.1$ K. For one single estimation, one obtains after minimization $\hat{U} = 9.989 \ 10^{-4}$ (m/s) and $\hat{h} = 9.899$ (W.m^{-2}.K^{-1}). The rms residual between the temperature profile on the hot face $T_h(x)$ and the simulated profile $T_h\left(x_i; \hat{U}, \hat{h}\right)$ is of the same order magnitude as the standard deviation of the added noise.

To quantify the quality of the estimation procedure, one can calculate the variance-covariance matrix defined by:

$$cov\left(\hat{\beta}\right) = \sigma_t^2 \left(\boldsymbol{S}^T \boldsymbol{S}\right)^{-1} \tag{17}$$

where $\boldsymbol{S}$ is the sensitivity matrix and $\beta = [U, h]^T$ is the parameter vector. This covariance matrix has diagonal elements which are the variances of $\hat{\beta}_j$'s. They characterize the dispersion (standard deviation) of the estimation $\hat{\beta}$ of parameter β around the expectation of the estimator:

U	relative standard deviation $\sigma_{\hat{U}}/U$	relative standard deviation $\sigma_{\hat{h}}/h$
10^{-3}	2.87×10^{-2}	12.9×10^{-2}
10^{-4}	0.46×10^{-2}	0.48×10^{-2}
10^{-5}	2.06×10^{-2}	0.25×10^{-2}

Table 3. Relative standard deviation for the covariance matrix.

To verify this results, one carries out several tests of inversion with $N_s = 100$ realizations of the added noise. The results in terms of the averages of the N_s estimations are given in table 4.

U	$\bar{\hat{U}}$	$\sigma_{\hat{U}}/U$	$\bar{\hat{h}}$	$\sigma_{\hat{h}}/h$
10^{-3}	9.9837×10^{-4}	2.4518×10^{-2}	10.1454	8.480×10^{-2}
10^{-4}	9.994×10^{-5}	0.402×10^{-2}	9.9969	0.46×10^{-2}
10^{-5}	1.0009×10^{-5}	1.9625×10^{-2}	10.0013	0.25×10^{-2}

Table 4. Evolution of the estimation results of U and h with the mean velocity U.

All these results show that both parameters can be estimated using measured temperatures.

3.2. Estimation of the boundary conditions at the internal walls
One uses here the analytical model (11) combined with the temperature of the external faces and with the external coefficient of exchange h previously estimated in order to estimate internal wall temperature T_{wh} and T_{wc} and internal wall fluxes φ_{wh} and φ_{wc}. It is an inverse heat conduction problem where the wall temperature profile and flux on both external faces of the system are considered as data (input). By writing now the quadripolar relationship (11) between the hot face and the internal hot wall, one obtains:

$$\begin{bmatrix} \theta_n \\ \Phi_n \end{bmatrix}_h = \boldsymbol{H}_1 \boldsymbol{S}_{1n} \begin{bmatrix} \theta_n \\ \Phi_n \end{bmatrix}_{wh} \quad \text{therefore} \quad \begin{bmatrix} \theta_n \\ \Phi_n \end{bmatrix}_{wh} = (\boldsymbol{H}_1 \boldsymbol{S}_{1n})^{-1} \begin{bmatrix} \theta_n \\ \Phi_n \end{bmatrix}_h \tag{18}$$

Thus starting from the simulated noisy temperature and the known flux on the hot face, one can estimate the Fourier transform of temperature and flux $\begin{bmatrix} \theta_n \\ \Phi_n \end{bmatrix}_h$ for $N_h' \leq N_h$ harmonics

(parametrization of the data using model (13)) and afterwards deduce the boundary conditions at the internal hot wall $T_{wh}(x)$ and $\varphi_{wh}(x)$ by (18). For the cold wall, one can write in a similar manner:

$$\begin{bmatrix} \theta_n \\ \Phi_n \end{bmatrix}_{wc} = \boldsymbol{S}_{2n}\boldsymbol{H}_2 \begin{bmatrix} \theta_n \\ \Phi_n \end{bmatrix}_c \tag{19}$$

In figure 5, one plots the noisy temperature profile of the external hot face T_h (pseudo-experiment with $\sigma = 0.1$ °C) and the parametrized temperature profile obtained with $N_h = 12$ harmonics and also the corresponding temperature residual. The results of the estimation of the internal walls boundary conditions for $U = 10^{-5}$ (m/s) are now considered. Figure 6 shows the temperature profiles obtained by the analytical model (18) T_{wh} for $N_h = 100$ and by inversion of (18) using the previously parameterized external T_h profile ($N_h = 12$). The difference (error) between these profiles is also shown on the same figure. The fluxes over external walls (φ_h and φ_c) and internal wall (parametrized φ_{wh} and φ_{wc} and estimated $\hat{\varphi}_{wh}$ and $\hat{\varphi}_{wc}$) are given in figures 7 and 8 (cold face temperature distribution is simulated the same way).
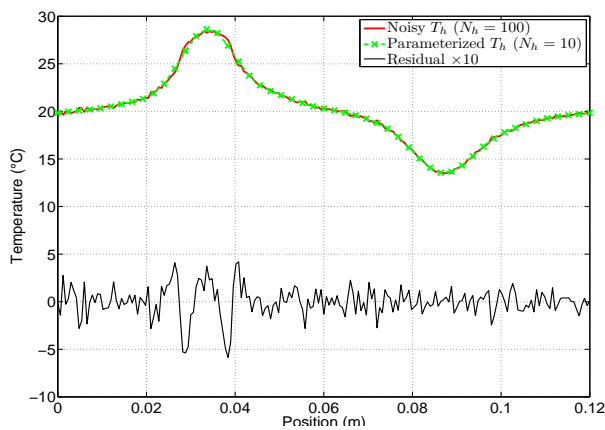

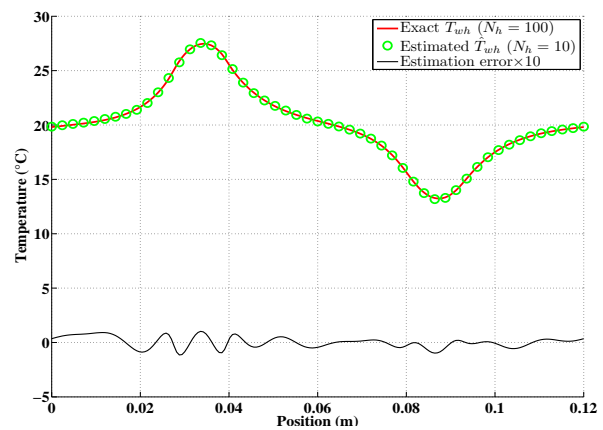**Figure 5.** Noisy and parametrized temperatures of the external hot face for $U = 10^{-5}$ (m/s).

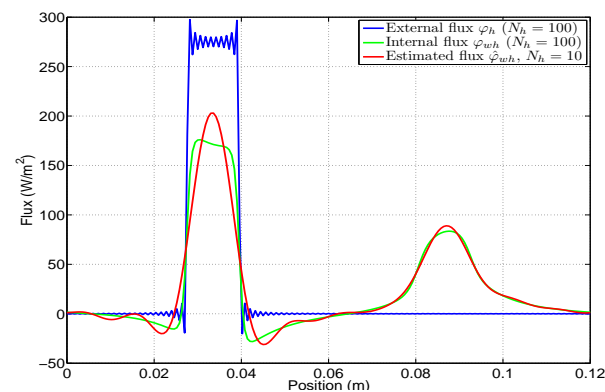**Figure 6.** Estimated temperature on the internal hot wall for $U = 10^{-5}$ (m/s).

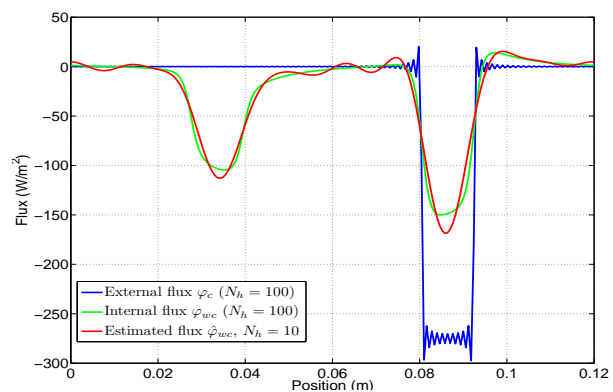**Figure 7.** External hot flux (φ_h) and internal hot wall fluxes (φ_{wh} and $\hat{\varphi}_{wh}$).

Figure 8. External cold flux (φ_c) and internal cold wall fluxes (φ_{wc} and $\hat{\varphi}_{wc}$).

3.3. Calculation of the bulk temperature

The final objective of this work is to shortcut the notion of internal heat transfer coefficient to recover the bulk temperature $T_b(x)$ of the flow directly through a thermal balance in the liquid. We show here how to get a model for it. In 2D channel flow, the bulk temperature $T_b(x)$ is defined by:

$$T_b(x) = \frac{1}{U e_f} \int_0^{e_f} u(y) T(x, y) \, \mathrm{d}y \tag{20}$$

Using the decomposition of the fluid layer into K sub-layers previously used to make the velocity field uniform in each layer, one obtains:

$$T_b(x) = \frac{1}{U e_f} \sum_{k=1}^{K} \int_{e_{k-1}}^{e_k} u_k \, T_k(x) \, \mathrm{d}y \tag{21}$$

therefore:

$$T_b(x) = \frac{1}{U e_f} \sum_{k=1}^{K} u_k \, T_k(x) \, e_k \tag{22}$$

where $T_k(x)$ will be calculated the same way the wall temperatures by using the analytical model:

$$\begin{bmatrix} \theta \\ \Phi \end{bmatrix}_{y_k} = \left(\boldsymbol{H}_1 \boldsymbol{S}_{1n} \left(\prod_{j=1}^{k} (\boldsymbol{F}_{kn}) \right) \right)^{-1} \begin{bmatrix} \theta \\ \Phi \end{bmatrix}_h \tag{23}$$

4. Conclusion and perspectives

The objective of this preliminary study is a numerical modelling of the flow and heat transfer in a plane mini-channel with a validation of the modelling through an experiment bench where the distribution of the temperature is measured by an infrared camera. An analytical model has been presented. It uses Fourier transforms that allow the calculation of the conjugated heat transfer inside a mini-channel without the use of any internal heat transfer coefficient. A sensitivity analysis of the external wall temperature distribution to the velocity profile and to the external heat transfer coefficient has been implemented, as well as the inversion of external 1D temperature fields. They showed that experimental implementation of this method was possible. The next stage will consist to the experimental validation by using the model developed in this study and the infrared thermography in an inverse approach.

References

[1] G.L. Morini. Single-phase convective heat transfer in microchannels: A review of experimental results. *International Journal of Thermal Sciences*, 43, Issue 7:631–651, 2004.
[2] G. Maranzana, I. Perry, and D. Maillet. Mini and micro-channels: influence of axial conduction in the wall. *International Journal of Heat and Mass Tranfert*, 47:3993–4004, 2004.
[3] Kevin D. Cole and Barbaros Cetin. The effect of axial conduction on heat transfer in a liquid microchannel flow. *International Journal of Heat and Mass Transfer*, 54:2542 – 2549, 2011.
[4] I. Perry, Y. Jannot, D. Maillet, and B. Fiers. Effect of velocity distribution on external wall temperature field for a flat microchannel,. *Experimental Heat Transfer*, 23:27–43, 2009.
[5] D. Maillet, S. André, J.C. Batsale, A. Degiovanni, and C. Moyne. *Thermal quadrupoles: solving the heat equation through integral transforms.* Wiley, 2000.
[6] Comsol multiphysics version 3.4.
[7] The mathworks matlab natick, ma (2011) http://www.mathworks.com.